Crystal growth, structural, optical, thermal and non-linear optical response of L-serine doping in potassium sulphato oxalate single crystals

G. Durgababu[1], Y. A. S. Anitha[2], I. Ramakanth[3], K. Srinivasa Rao[4], B. Lakshmanarao[5], R. Govindaraj[6], P. V. L. Narayana[2], and G. Bhagavannarayana[7,*]

[1] *Department of Physics, Rajiv Gandhi University of Knowledge Technologies, Nuzvid, Andhra Pradesh 521202, India*

[2] *Department of Nuclear Physics, Andhra University, Visakhapatnam, Andhra Pradesh 530003, India*

[3] *Department of Chemistry, School of Advanced Sciences, VIT-AP University, Amaravati, Andra Pradesh 522237, India*

[4] *Department of Physics, Government Degree College, Dr B. R. Ambedkar Konaseema District, Mandapeta, Andhra Pradesh 533308, India*

[5] *Department of Chemical Engineering, Rajiv Gandhi University of Knowledge Technologies, Nuzvid, Andhra Pradesh 521202, India*

[6] *SSN Research Centre, Sri Sivasubramaniya Nadar College of Engineering, Tamil Nadu, Kalavakkam 603110, India*

[7] *Department of Physics, VSM Group of Institutions, E.G. (Dt.), Ramachandrapuram, Andhra Pradesh 533255, India*

ABSTRACT

The novel non-linear optical materials of pure and L-serine (LS) doped potassium sulphato oxalate (KSO) single crystals at different concentration levels (1 mol%, 2 mol% and 3 mol%) are grown by conventional slow evaporation solution growth technique (SEST). The grown crystals were studied for their structural, optical, thermal and second harmonic generation (SHG) efficiency properties. The Powder X-ray diffraction (PXRD) spectrum confirms the grown crystals are triclinic crystalline system with space group *P1* for pure KSO and it remains unchanged for LS-doped KSO single crystals at different concentration levels except small angular shift for few intense peaks. As the doping concentration increases, the intensity of (201) peak increases due to the preferred orientation of c-axis and the absence of (−100), (−101) peaks. The presence of doped molecules was identified through infrared spectroscopy. The absorbance was decreased with increasing doping concentration and indirect band gap energy increased from 3.9 eV for pure KSO to 4.6 eV for 3 mol% LS-doped KSO which indicates that these materials are one of the best choices for efficient light conversion materials. The crystalline perfection of grown crystals was assessed by High-resolution X-ray diffraction (HRXRD) technique. At an optimum doping concentration, the crystalline perfection was increased due to predominant occupation of doped molecules at the sites of grain boundaries. The thermal stability of the samples was carried out using thermo gravimetric analysis (TGA) and differential thermal analysis (DTA) study. The sharp increase in photo luminescent intensity for 3 mol% LS-doped

Address correspondence to E-mail: bhagavanna55@gmail.com

🙅 Springer

KSO at 563 nm is preferable for green light fluorescence applications. The relative second harmonic generation (SHG) efficiency was increased with increasing doping concentration. At 3 mol% of LS doping, KSO crystals showed an enhanced efficiency by 1.45 times to that of standard KDP crystals. Thus, the grown crystals were found to have potential applications for optoelectronic device applications.

1 Introduction

The new class of organic and semiorganic based single crystals has gained much attention of many researchers in the field of non-linear optics (NLO) for the fabrication of different optoelectronic devices. Although the growth of inorganic based single crystals have critical issues like controllable growth, uniform orientation, identical thickness and also patterning in desired direction, the organic materials based optoelectronic devices exploits because of their intrinsic unique property of conjugated bonds among the molecules and the formation of extremely low density defects. And also, organic single crystals possess better NLO efficiency but shows poor in mechanical and thermal stability. Our recent studies on the growth of organic based single crystals showed better linear [1] and NLO properties for device fabrication [2, 3]. Growth of organic crystals with better SHG efficiency is in much demand because of their low cost of materials, simplicity in growth and ease of device fabrication. The recent developments of inorganic based single crystals exploits their applications in semiconductor industry because of their better mechanical and thermal stability but poorer NLO efficiency [4]. Most of the inorganic based single crystalline materials doped with a suitable dopant were used to tune their properties as well [5]. The routes of growing inorganic single crystals in different techniques also play a vital role for their excellent properties like laser damage threshold, mechanical strength, higher polarizability, wide transparency, because of their strong molecular or ionic boding nature of the inorganic materials. Therefore, in order to achieve better mechanical strength, thermal stability, excellent transmittance and higher NLO efficiency with flexible chemical interaction, one has to choose other phase of materials such as semiorganic materials. There are many reports on this class of materials which showed better optical, mechanical,

thermal properties [6–11]. In order to harmonize the properties of the host materials, the doping technique has been using extensively by many researchers across the globe in the field of crystal growth. The synthesis of doping compound into host materials alters its intrinsic properties such as lattice parameters, crystalline quality, optical transmittance window and NLO response because the dopant causes hybridization and initiating additionally obtainable electrons for conduction process [12]. This doping method also useful to alter the bang gap energies and the dopants can shift the fermi level and create impurity states [13]. The recent literature reports on pure and different amino acids doped semi-organic single crystals are extensively employed SEST method and reveal the improvement of their NLO efficiency and other physio-chemical properties for different optoelectronic and photonic device applications [14–20]. Most of the amino acids are zwitter ionic in nature and molecular chirality behaviour causes to strengthen the host material strength mechanically and thermally with wide transparency [21, 22]. ʟ-threonine doped potassium dihydrogen phosphate unidirectional grown single crystals showed better crystalline perfection without any structural grain boundary and red shift in its band gap energy with more than 80% of transmittance could replace the pure KDP single crystals for device applications [23]. Our recent reports on ʟ-Phe doped KDP crystals revealed interesting facts such as crystalline perfection which has not deteriorated up to an optimum value of doping concentration [24]. Our current research is on potassium sulphato oxalate (KSO) single crystal, a triclinic crystal system with space group P1. It is one of the semi-organic single crystals to grow by a low cost effective conventional SEST method and it has good laser damage threshold, mechanical and thermal stability than pure KDP [25]. Hence, it makes our interest to see its behaviour by means of doping with amino acids at different concentration levels.

Therefore, tuning the characteristics of KSO semi-organic single crystals with L-Serine (LS) dopants at varied concentration levels into the KSO crystalline matrix is quite interesting. The common observation in most of the amino acids is that the proton is transferred from the carboxylic group (COO^-) to the amino group (NH_3^+) resulting in the ionic character of the zwitterionic molecules. Among all the amino acids, L-Serine has a shorter side chain with bi-functional organic groups, *i.e.*hydroxymethyle group as shown in inset of Fig. 1. It provides many additional properties which are not common in other amino acids. This hydroxymethyle side chain provides high polarity and it can interact freely with water molecules or with the external environment. Therefore, it easily gets soluble with the polar solvents and can combine quickly with KSO compound. Therefore, in the present investigation, L-Serine doped KSO single crystals by SEST method were successfully grown and characterized for the first time to see their properties for different optoelectronic device applications.

2 Experimental: synthesis and crystal growth

The synthesis of pure KSO was made with the raw materials of potassium sulphate (minimum assay ~ 99%, AR grade) and oxalic acid (minimum assay ~ 99.5%, AR grade) are purchased from S D Fine-Chem Limited, Mumbai India. The saturated solution was prepared by taking these compounds in a stoichiometric ratio of 1:1 using deionized water. This saturated solution was re-crystallized and the solution was filtered with Wattman filter papers (dia ~ 125 μm) to remove the impurities present in the raw material and repeated the same process for 3 times. Finally, the synthesized pure KSO compound was obtained, when the prepared solution was dried on a heated plate at a temperature somewhat higher than the room temperature (RT). In slow evaporation solution growth technique (SEST), the super-saturated solution of pure KSO was prepared using deionized water at RT and kept in four beakers with 100 ml in each. In three beakers, 1 mol%, 2 mol% and 3 mol% concentration of LS compound was added as a dopant. The above dopant concentrations of LS compound were chosen because of its less molecular weight, i.e. 105.09 g/mol. To achieve the homogeneous saturated solution, the temperature was increased slightly by ~ 0.5 °C and then decreased back slowly to RT. The thus prepared solutions were covered with perforated aluminium foil with few fine holes to control the evaporation rate and then kept for slow evaporation for single crystal growth at RT. The crystallization took place in 20–30 days and harvested crystals are shown in the Fig. 1a–d.

3 Characterization techniques

The grown crystals were subjected to PXRD using Bruker Discover D8; with CuK_α radiation source of wavelength 1.5406 Å. The spectra were recorded within the angular range of $10^\circ \leq 2\theta \leq 90^\circ$ at a scan rate 0.3° min^{-1} at RT. UV–Vis-NIR spectroscopy studies
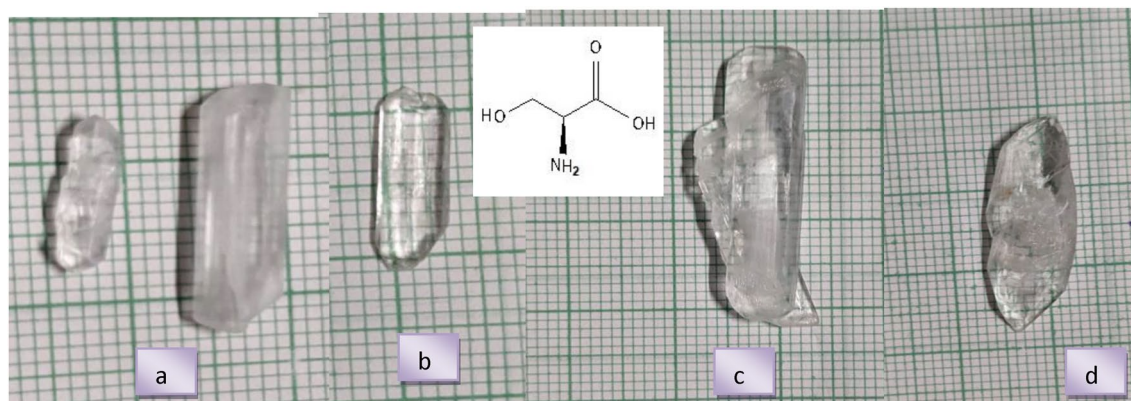
Fig. 1 Conventional SEST grown single crystals of **a** Pure **b** 1 mol% **c** 2 mol% and **d** 3 mol% concentrations of LS-doped KSO (the inset shows the molecular structure of L-Serine (LS) dopant)

were made using CECIL 7400 Double-beam spectrometer in the wavelength range of 200 nm–1100 nm at a scan rate of 200 nm/min with slit width of 5 nm. Fourier transform Infrared (FT-IR) Spectroscopy was performed using Bruker, USA, Alpha T Model. The transmittance spectrum was recorded at room temperature within the limit of wave number range of 500–4000 cm^{-1} with spectral resolution 1 cm^{-1}. Photoluminescence spectra were recorded for grown crystals using F-7000 FL-Spectrophotometer at RT. The excitation wavelength 280 nm was chosen for the samples and scanned in the range of 350–700 nm with a scan speed of 1200 nm/min. The slit width for both the excitation and emission spectra were fixed at 5 nm. High-Resolution X- ray Diffractometry (HRXRD) using a PANalytical X'Pert PRO MRD system with $CuK\alpha_1$ radiation was employed to assess the crystalline perfection of bulk grown crystal specimens. The thermal stability and mass loss of the samples were measured using TGA and DTA analyses. Kurtz powder technique [26] was employed to determine the relative performance of the SHG efficiency among the pure and doped specimens using Q-switched Nd: YAG laser (1064 nm. Quanta ray Series, USA) set at 10 ns pulse duration with frequency repetition rate of 10 Hz. These experimental techniques are well described in our recently published article [24].

4 Results and discussions

4.1 PXRD analysis

The powder x-ray diffraction study was preferred to understand the structural stability of grown pure and LS-doped KSO single crystals at different doping concentrations. The obtained XRD spectra of grown crystals shown in Fig. 2 were compared with the already reported single crystal XRD spectra with $MoK\alpha$ radiation ($\lambda = 0.71073$ Å) obtained for pure KSO [25]. The unit cell parameters and volume of the unit cell (V) of grown crystals were refined using checkcell software and obtained values were shown in Table 1. The obtained refined data showed that the crystalline system is triclinic with space group *P1* and remains unchanged for LS doping at all concentrations. The calculated (hkl) indices of the corresponding reflecting Bragg planes were indexed as shown in Fig. 2.

From the data, the lattice constants and unit cell volume almost remain unchanged with LS doping
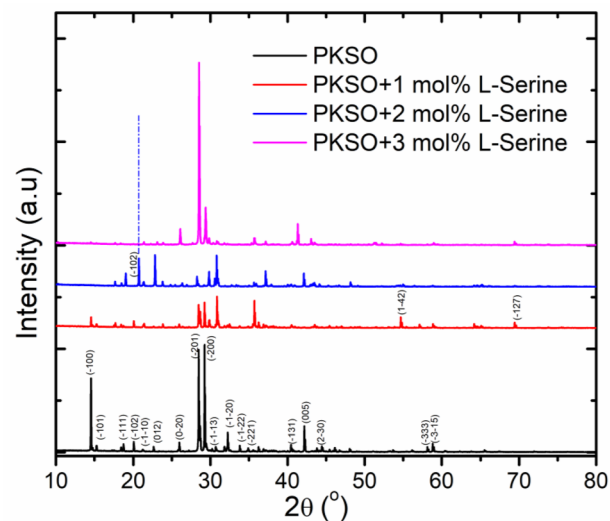
Fig. 2 Powder XRD pattern of pure and 1, 2 and 3 mol% concentrations LS- doped KSO crystals

in KSO single crystals [25]. This indicates that the doped LS molecules occupied the interstitial sites of the KSO crystal. The increased intensity of the (201) peak for 3 mol% LS-doped KSO single crystal indicates preferred growth along the c-axis [3]. And it is our interest to see the crystalline perfection of the same plane which was discussed more elaborately in the forthcoming Sect. 4.4. The peaks observed in the pure KSO specimen (− 100), (− 101) at $2\theta = 14.53°$ and $15.24°$, respectively, were nearly absent in the doped specimen at higher doping concentrations, i.e. at 3 mol% of LS-doped KSO crystals. It is due to the reason that LS compound predominantly induced into the absented (− 100), (− 101) planes due to the strong interactions between the proton donating and accepting groups of amino acids (NH^+) in ʟ -serine and carboxylic acid groups (COO^-) in oxalic acid. The sharp and intense peak observed for (-201) at higher doping concentration levels suggests good crystalline perfection as revealed in HRXRD studies described in Sect. 4.4.

4.2 FT-IR studies

The pure KSO and LS- doped KSO single crystals at different concentrations were subjected to FT-IR spectroscopy in the wave number range from 600 to 4000 cm^{-1} using KBr pellet technique to identify the functional groups present in the grown specimens and it is depicted in Fig. 3. To observe more clearly the functional groups at lower wave numbers present in

Table 1 Refined unit cell parameters of pure KSO and LS-doped KSO using chekcell software

Parameters	Reported pure KSO [25]	Refined pure KSO	1 mol% LS-doped KSO	2 mol% LS-doped KSO	3 mol% LS-doped KSO
a (Å)	6.37	6.364(7)	6.341(5)	6.363(1)	6.376(7)
b (Å)	7.03	7.170(1)	7.014(8)	7.013(2)	6.937(4)
c (Å)	10.61	10.592(3)	10.615(9)	10.627(9)	10.612(3)
V (Å)^3	456	455.7(1)	455.3(5)	453.2(1)	449.1(2)

Fig. 3 FTIR spectrum **a** 600–4000 cm^{-1} and **b** 600–2000 cm^{-1} of pure KSO and 1, 2 and 3 mol% concentrations of LS-doped KSO crystal
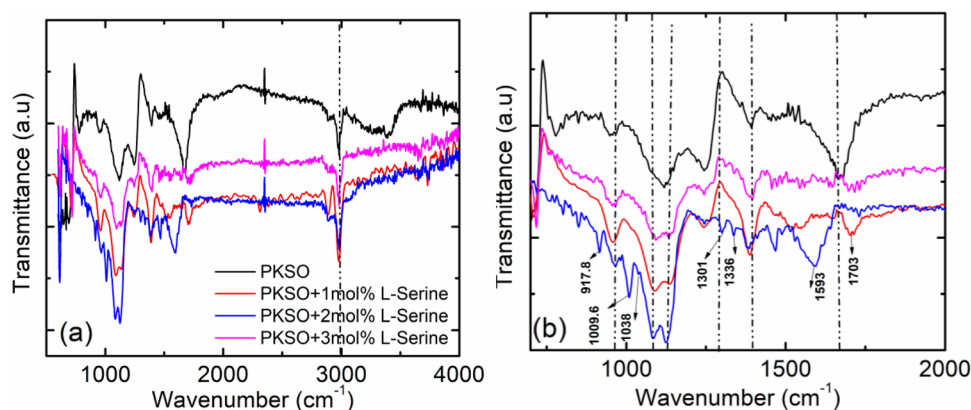
the spectrum, it was redrawn as a separate spectrum between 500 and 200 cm^{-1} and shown in Fig. 3b. The O–H band observed at 1401 cm^{-1} in pure KSO [25], was slightly shifted to higher wave number regions 1405, 1407 and 1410 cm^{-1} in the case of 1 mol%, 2 mol% and 3 mol% concentrations of LS-doped KSO crystals, respectively. It indicates the presence of carboxylic groups, which were predominately occupied in the KSO matrix. The shifting of IR band is prominent at higher doping concentrations i.e. at 3 mol% as expected.

The C–C stretching bond was assigned to the peaks at 916, 916 and 917.8 cm^{-1} for the 1 mol%, 2 mol% and 3 mol% concentrations of LS-doped KSO crystal, respectively [27]. CH$_2$ stretching band was observed at 1009 cm^{-1} in only 3 mol% LS-doped KSO single crystals [27]. The symmetric S=O stretching was assigned for pure KSO at 1124 cm^{-1} [25] while it was shifted to 1127 cm^{-1} for LS-doped KSO at all 1 mol%, 2 mol% and 3 mol% concentration levels. Similarly, S–O–H plane bending was also observed at 1120 cm^{-1} for pure KSO [25] while it was shifted to 1121 cm^{-1} for 1 mol%, 2 mol% and 3 mol% doping concentrations of LS in KSO crystals. The C–H bending was observed for pure KSO at 1471 and 790 cm^{-1} [25], which were slightly shifted to 1468 cm^{-1} and 796 cm^{-1} in all LS-doped KSO crystals. The peak corresponding to LS dopant at 1301 cm^{-1} corresponding to C–H symmetric

stretching was observed only in 3 mol% concentration sample [27]. The strong intensity vibration band at 1684 cm^{-1} is attributed to C=O absorption band with asymmetric stretching of COO– for pure KSO while it was shifted significantly to 1701 cm^{-1} in 3 mol% LS-doped KSO crystal. The intense peak observed at 3424 cm^{-1} is assigned to O–H stretching vibration of hydrogen bonds in pure KSO, which was shifted to 3418 cm^{-1} at all the experimental concentration levels of LS in KSO. The assignments of molecular vibrations for corresponding wave numbers measured in cm^{-1} obtained from the experiment are shown in Table 2.

4.3 UV–Vis-NIR spectral analysis

Figure 4a, shows the UV–Vis-NIR spectrum of pure crystals and LS-doped crystals at 1 mol%, 2 mol% and 3 mol% concentrations. The optical absorbance of the grown crystals decreased during the spectral range from 400 to 1100 nm and the cut–off wavelengths also found to be decreased due to doping. The cut–off wavelengths were measured from Fig. 4a. For pure KSO it is 310 nm and for doped KSO at 1 mol%, 2 mol% and 3 mol% LS concentrations the values are 305 nm, 297 nm, 274 nm, respectively. This blue shift in cut-off wavelength, which is highest at 3 mol% LS doping is favourable for the NLO activity. The band gap energies were measured using the following

Table 2 FTIR assignments of the pure potassium sulphato oxalate (KSO) and LS-doped KSO crystals at different concentration levels (i.e. 1 mol%, 2 mol% and 3 mol%)

Assignments of molecular vibrations	Pure KSO (cm^{-1})	1 mol% LS-doped KSO (cm^{-1})	2 mol% LS-doped KSO (cm^{-1})	3 mol% LS-doped KSO (cm^{-1})
O–H stretching	3424	3418	3418	3418
C=O band/γ_{as} COO$^-$	1684	1686	1687	1703
C–H bending	1471	1468	1468	1468
O–H due to carboxylic	1401	1405	1407	1410
C–H symmetric stretching	–	–	–	1301
S–O–H plane bending	1220	1221	1221	1221
Symmetric S=O stretching	1124	1127	1127	1127
C–C stretching	–	916	916	917.8
CH$_2$ rocking	–	–	–	1009
C–H bending	790	796	796	796
C–C stretching/γ_{as} SO$_4$	720	720	719	718

Fig. 4 **a** Optical absorbance spectrum and **b** band gap energy spectrum of pure KSO and 1, 2 and 3 mol% concentrations of LS-doped KSO crystal
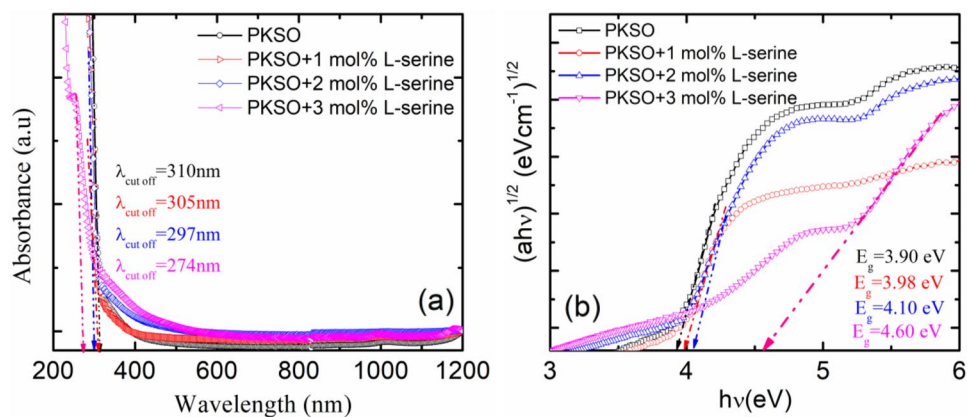
relation from the experimentally obtained absorption co-efficient (α) [3, 28],

$$(\alpha h v)^n = A\left(h v - E_g\right) \qquad (1)$$

where A is an arbitrary constant and if $n = \frac{1}{2}$, the above equation is valid for indirect transitions and $n = 2$ for direct transitions, h–plank's constant and v- frequency of the incident photons and E_g is the optical band gap energy. The linear portion of the curve extrapolated to zero absorption was well fitted to the indirect optical band gap nature and hence the values were obtained from the plot of $(\alpha h v)^{1/2}$ against "$h v$" as in Fig. 4b. The band gap (Eg) was found to be 3.9 eV for pure KSO while 3.98 eV, 4.1 eV and 4.6 eV were obtained for LS-doped KSO crystals, respectively, for 1 mol%, 2 mol% and 3 mol% concentrations. As the band gap energies of the grown crystals more than 2 eV are treated as wide band gap (WBG) materials which have properties lie between the semiconductors and insulators

such as high critical electric field density, frequencies and high thermal stability [29]. WBG energy materials have garnered significant interest in several sectors such as photonics, optoelectronics and spintronics. [30]. WBG's allow devices to switch larger voltages and bring the electronic transitions in the frequency range of visible regions or even produce ultraviolet radiations [29]. Therefore, the grown samples are suitable for better light conversion efficiency which makes these crystals a good choice for fabrication of optoelectronic devices like LED's and laser diode semiconductor materials.

4.4 High-resolution XRD analysis

Figure 5 shows the high-resolution diffraction or rocking curve (RC) recorded for pure and LS-doped KSO single crystals for (201) diffracting planes. As seen in Fig. 5a, the high-resolution RC is quite sharp without any satellite peaks due to the absence of any internal

Fig. 5 a Diffraction curve recorded for pure KSO single crystal. The plots **b**, **c** and **d** are, respectively, for LS-doped crystals at 1, 2 and 3 mol% concentrations recorded for (201) diffracting planes by employing the X'Pert PRO MRD X-ray diffractometer with CuKα₁ radiation in Bragg symmetrical Bragg geometry. The inset in **c** depicts the compression of lattice close to the defect core due to interstitial point defect. The inset in f **d** depicts the very low angle structural grain boundary responsible for the satellite peak at the lower Bragg diffraction angle of the RC
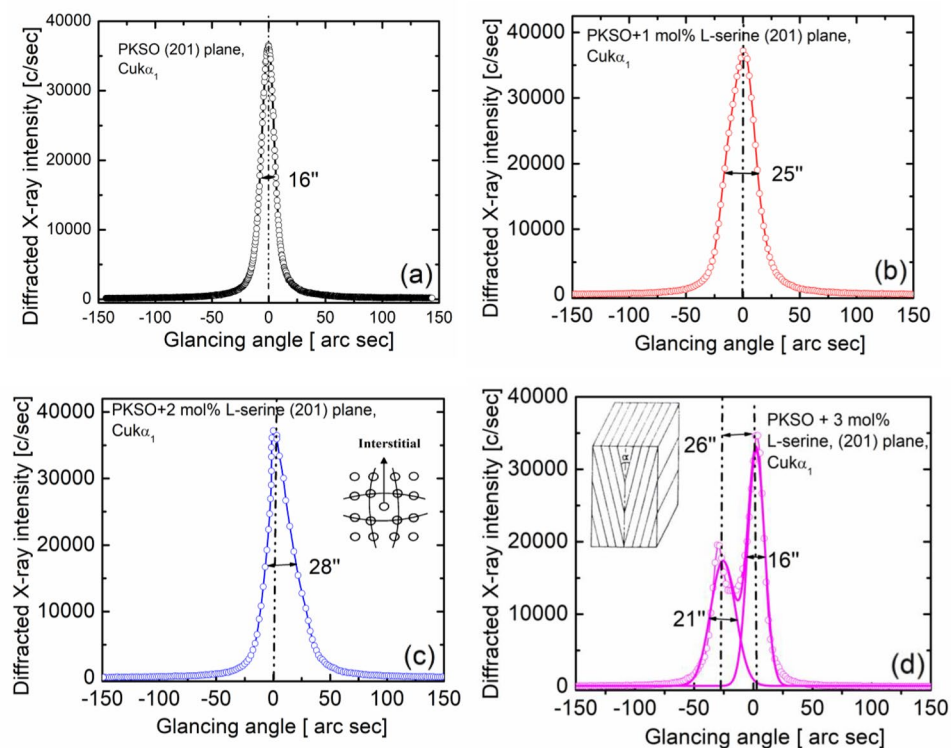
structural grain boundaries. The full width at half maxima (FWHM) of the RC of pure KSO [Fig. 5a] is 16 arc sec, which is very close to that expected from the plane wave dynamical theory of X-ray diffraction [31]. The crystals which showed this characteristic behaviour such as the single sharp diffraction curve with low FWHM indicates the crystalline perfection is quite good [31].

Figure 5b shows the RC for a typical 1 mol% LS-doped KSO single crystal specimen using (201) diffracting planes recorded under identical conditions as that of Fig. 5a. The FWHM of the main peak is 25 arc sec without any additional peak(s) showing the absence of low angle and very low angle grain boundaries which indicates the crystalline perfection is good but due to doping, the FWHM slightly increased from 16 to 25 arc sec. In case of the Fig. 5c corresponding to doping level at 2 mol%, the FWHM is further increased from 25 to 28 arc sec. In this curve, it is interesting to note the shape of the curve with respect to the exact Bragg peak position, which is not symmetric when compared to Fig. 5a and b. This indicates the fact that the crystal lattice at the defect core at higher concentrations leads to compressive stress [as depicted in the inset of Fig. 5c] resulting in reduced lattice constant 'd' around the defect core leading to

more scattered intensity (from local Bragg diffracted intensities of the lattice around the interstitially occupied dopants) along the wings of the diffraction curve at higher Bragg angles. This is well understood from the fact that in the Braggs' diffraction equation, i.e. $2d\sin\theta = n\lambda$, when '*d*' decreases, the Bragg angle θ increases [3, *G. Durgababu & G. Bhagavannarayana et.al (2021)*]. The asymmetry in Fig. 5b is not that visible due to the relatively lower concentration of dopants.

Figure 5d shows the RC recorded for the sample with 3 mol% doping of LS in KSO single crystal. This DC is different from that of Fig. 5a–c with an additional peak (with FWHM value of 21 arc sec) at an angle of 26 arc sec away from the main peak (with FWHM value of 16 arc sec) and depicts the presence of a very low angle boundary as the misorientation angle α is less than one arc min [31]. This RC has some interesting features. The FWHM of the main peak is the same as that of the undoped KSO crystal and depicts good crystalline quality. The FWHM of the additional peak is 21 arc sec. This value is also small enough as expected for nearly perfect crystals [32]. As observed in our earlier investigation about the dynamic nature of point defects on KDP crystal grown by temperature lowering method [33], in this sample at a higher concentration of 3 mol%, initially during the growth the

dopants entered into the crystalline matrix at interstitial sites. Due to self-generated compressive stress, a very low angle boundary (a microstructural disorder) had been formed and the dopants seem to be segregated along the boundary. Since these are microscopic defects, the macroscopic properties do not really affect much, yet the benefit of doping has been achieved in the crystals exhibited by the bulk crystals as we have seen in the present studies.

4.5 TGA-DTA analysis

The thermal properties and mass loss were studied for pure and LS-doped KSO grown crystals at different concentrations (1 mol%, 2 mol% and 3 mol%). The grown samples are made into fine micron sized powder samples. Approximately ~ 13.5 mg weight of powder samples was used for TG–DTA in nitrogen atmosphere in the temperature range from 20 to 600 °C. The heating rate was of the order of ~ 10 °C min^{-1}. The sample was taken in an alumina crucible during the measurements. The obtained thermo gravimetric (TG)-differential thermo gravimetric (DTG) curves showed in the Fig. 6a–d are for pure, and 1 mol%, 2 mol% and 3 mol% LS-doped KSO samples, respectively. It is seen from Figs. 6a–c, the weight loss occurs in five stages

while in case of Fig. 6d the weight loss occurred only in one stage. Initially there was no weight loss up to 100.3, 83, 83 and 217.5 °C in pure, 1 mol%, 2 mol% and 3 mol% concentrations of LS-doped KSO crystals, respectively. The first gradual weight loss at 6.35%, 1.707%, 3.08% occurred in the temperature ranges between 100.3 and 136.3, 83 and 134 and 83 and 160.45 °C is assigned to the loss of water at endothermic peak of DTG curve at 106.2, 106.2 and 86.7 °C, respectively, for pure [25], 1 mol% and 2 mol% LS-doped KSO single crystals. The second significant weight loss occurred in the samples in TG curve at 7.51%, 3.48% and 2.72% in between 136.3 and 181.84 °C, 134 and 179.05 °C, 186.156 and 160.45 °C are due to the release of gaseous products like CO, CO_2 in association with small endothermic peak at 182, 182 and 188 °C that corresponds to the melting point of the KSO crystal in pure [25], 1 mol% and 2 mol% concentrations of LS-doped KSO grown crystals, respectively.

The third weight loss of about 12.47%, 5.28% and 5.18% % in TG curve occurring between 181.84 and 197, 179 and 255 and 186 and 256 °C are due to major decomposition and volatilization of the material which is endothermic at about 199, 255, 256 and 216 °C for pure, 1 mol%, 2 mol% and 3 mol% concentrations of LS-doped KSO grown crystals, respectively. The final

Fig. 6 TGA–DTA curves of **a** Pure **b** 1 mol% LS **c** 2 mol% LS and **d** 3 mol% LS-doped KSO single crystals
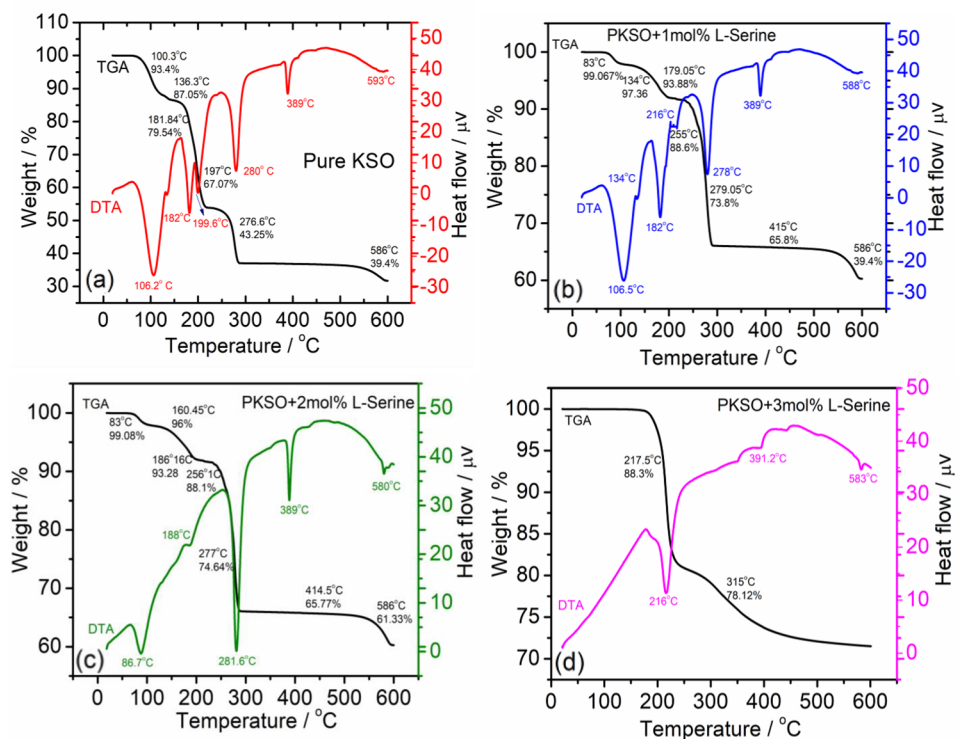
decomposition of the samples weight loss of 27.67%, 34.4%, 13.31% and 10% was occurred between 276 and 586, 278 and 586, 277 and 586 and 217 and 315 °C for pure [25], 1 mol%, 2 mol% and 3 mol% concentrations of LS-doped KSO grown crystals, respectively. The small leftover fraction of the material is the residue of potassium oxide [34]. The irreversible endothermic peaks are attributed at 280, 389 and 580 °C for pure KSO, 278, 389 and 588 °C for 1 mol% LS-doped KSO crystals, 281, 389 and 580 °C for 2 mol% LS-doped KSO crystals and 281, 391 and 583 °C for 3 mol% LS-doped KSO crystals. The observed single phase transition in 3 mol% LS-doped KSO crystals with less weight loss between 217 and 315 °C is due to the special arrangement of dopants along the low angle grain boundaries as observed in HRXRD results. The high melting points and decomposition at higher temperatures of LS-doped KSO crystals arise probably because of the stronger bonding that exists between an oxalate molecule and a metal ion with L-serine dopant molecules [35].

4.6 PL analysis

The luminescence spectrum obtained whenever the light of photon with sufficient energy is used to excite some of the electronic states of a material. Due to the relaxation of the material from exited state to the ground state after a particular time interval, the material emits radiation. In the current study, the PL spectrum was recorded for pure KSO and LS-doped KSO crystals at room temperature (RT). Since, 3 mol% concentration of LS-doped KSO was found to have a lower cut-off wavelength around 274 nm, a lower excitation wavelength of 280 nm was chosen for all the samples. And hence the emission spectra could be recorded in the range of 350–700 nm. However, in the Fig. 7, the spectra were given in the useful range of 520–600 nm.

From the spectrum, only one emission peak was observed at 565 nm for both pure and LS-doped KSO single crystals at all concentrations. The intensity is distinctly higher for 3 mol% LS-doped KSO crystals due to the higher rate of recombination between the amino acid groups in doped specimen with carboxylic acid groups in oxalic acids of KSO crystalline matrix as observed in Sect. 4.2. The intensity of a single sharp intense peak at 3 mol% LS-doped KSO specimen confirms the better crystalline quality and indicates that the grown crystals at such higher concentration of
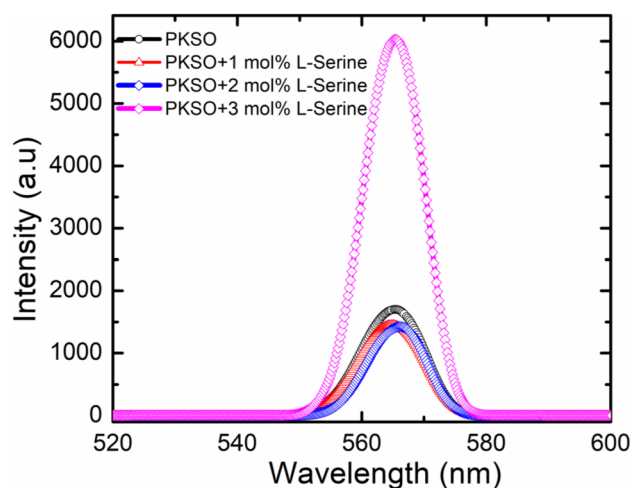
Fig. 7 Luminescence spectrum of pure KSO and 1, 2 and 3 mol% concentrations of LS-doped KSO crystals

Table 3 Comparison of SHG efficiency

Sample	SHG efficiency in comparison with pure KDP
Pure KDP	1
Pure KSO	1.22
1 mol% LS-doped KSO	1.25
2 mol% LS-doped KSO	1.34
3 mol% LS-doped KSO	1.45

doping cause green light fluorescence applications [24]. However, such enhanced properties can only be expected so long as the crystalline quality does not deteriorate, which is quite possible when the doping concentration is higher than a critical concentration [24]. Indeed, in our preliminary studies, when the dopant concentration was higher than 3 mol%, good crystals could not be obtained to subject them to characterization studies. Therefore, around 3 mol% of LS is to be treated as the optimum value of dopant level and well suitable for optoelectronic applications.

4.7 SHG efficiency

The SHG conversion efficiency of pure KSO, 1 mol%, 2 mol% and 3 mol% LS-doped KSO samples was found, respectively, 1.22, 1.25, 1.34 and 1.45 times to that of SHG of pure KDP standard sample as shown in Table 3. The cloud movement of π- electron from donor to acceptor leads to high polarization

to molecules. High polarization and intermolecular charge transfer are highly responsible for the enhancement of SHG efficiency and this increase in SHG efficiency with increasing doping concentration also observed in our earlier reports [24]. These present results reveal the enhancement of SHG efficiency with LS doping in KSO single crystals and found suitable for NLO device applications.

5 Conclusion

The pure and LS-doped KSO single crystals at different concentrations were grown successfully by the simple and economical SEST method. The PXRD spectrum confirms that the grown crystals are triclinic crystalline system. It remains unchanged for LS-doped KSO single crystals at different concentrations. FTIR confirmed the presence of the doped molecules in the KSO crystalline matrix. HRXRD revealed interesting features about the crystalline perfection in LS-doped KSO single crystals. The gradual increase in the value of FWHM due to increased doping level and the asymmetry in the high-resolution RC revealed that the dopants occupied the interstitial positions. However, at the highest possible doping level of 3 mol%, the self-driven compressive stress introduced in the lattice led to a microscopic very low angle boundary. However, the crystalline perfection of the main crystalline block improved and the dopants uniformly segregated along the grain boundary. The indirect band gap energies obtained from UV–Vis-NIR spectroscopic studies revealed that the grown crystals are suitable for efficient light conversion device applications. TG–DTA curves revealed the thermal stability needed for device applications. The PL fluorescence spectra revealed that the crystalline quality at higher doping concentrations is in good coherence with HRXRD results and the grown crystals at optimum doping concentration are good for fluorescent green light emission applications. The increased relative SHG efficiency at 3 mol% concentration of LS-doped KSO was obtained up to 1.45 times with that of the KDP crystals, which is another important finding in this class of semi-organic single crystalline materials. Therefore, the present studies revealed that the doping into the host compounds, helps in tailoring band gap energies and good non–linear optical response while maintaining the thermal stability and crystalline perfection within the range

of studied doping concentration, which suggests that the grown crystals have a wide range of optoelectronic and NLO applications.

Author contributions

All authors contributed to the study conception and materials properties. For the material synthesis and design of the experimental work and collection of data and analysis performed by [G Durgababu] [YAS Anitha] [I Ramakanth] [B. LakshmanaRao] [K.Srinivasa Rao], [T Kamalesh] [G Bhagavannnarayana] and [P.V. LakshmiNarayana]. The first draft of the manuscript written by [G Durgababu] and authors are read and approved the manuscript.

Data availability

The data used for analysis part of the manuscript during the current study will be made available by the corresponding author on reasonable request.

Declarations

References

1. G. Durgababu, G. Bhagavannarayana, T. Kamalesh, R. Govindaraj, G.J. Nagaraju, A comparative study of 4-chloro 3-nitro benzophenone crystals grown by slow evaporation solution and Sankaranarayanan-Ramasamy methods. J. Mater. Sci. Mater. Electron. **33**, 7973–7982 (2022)

2. G. Durgababu, G.J. Nagaraju, G. Bhagavannarayana, Effect of 2,4-dinitrophenol dye doping on tristhioureazinc(II) sulfate single crystals: a potential nonlinear optical material". J. Appl. Cryst. **53**, 972–981 (2020)

3. G. Durgababu, G.J. Nagaraju, G. Bhagavannarayana, Effect of malachite green dye doping in tristhiourea zinc (II) sulphate single crystal—a potential nonlinear optical material. J. Mater. Sci. Mater. Electron. **32**, 2564–2578 (2021)

4. P. Karuppasamy, V. Sivasubramani, M. Senthil Pandian, P. Ramasamy, Growth and characterization of semi-organic third order nonlinear optical (NLO) potassium 3,5-dinitrobenzoate (KDNB) single crystals. RSC Adv. **6**, 109105–109123 (2016)

5. J. Podder, The study of impurities effect on the growth and nucleation kinetics of potassium dihydrogen phosphate. J. Cryst. Growth **237**, 70–75 (2002)

6. G. Ramasamy, G. Bhagavannarayana, S. Meenakshisundaram, The concentration effects of s-, p-, d- and f-block element doping on the growth, crystalline perfection and properties of KDP crystals. Cryst. Eng. Commun. **14**, 3813–3819 (2012)

7. M. Shkir, V. Ganesh, N. Vijayan, B. Riscob, A. Kumar, D.K. Rana, M.S. Khan, M. Hasmuddin, M.A. Wahab, R.R. Babu, G. Bhagavannarayana, Analysis on structural, SHG efficiency, optical and mechanical properties of KDP single crystals influenced by glycine doping. Biomol. Spectrosc. **103**, 199–204 (2013)

8. B. Rsicob, M. Shakir, N. Vijayan, G. Bhagavannarayana, Effect of Mn(II) doping on crystalline perfection, nonlinear, optical and mechanical preoperties of KDP single crystals. Appl. Phys. A **107**, 477–484 (2012)

9. G. Bhagavannarayana, R.V. Ananthamurthy, G.C. Budakoti, B. Kumar, K.S. Bartwal, A study of the effect of annealing on Fe-doped LiNbO$_3$ by HRXRD, XRT and FT–IR. J. Appl. Cryst. **38**, 768–771 (2005)

10. G. Bhagavannarayaana, S.K. Kushwaha, Enhancement of SHG efficiency by urea doping in ZTS single crystals and its correlation with crystalline perfection as revealed by Kurtz powder and high-resolution X-ray diffraction methods. J. Appl. Cryst. **43**, 154–162 (2010)

11. G. Bhagavannarayana, S. Parthiban, S. Meenakshisundaram, Enhancement of crystalline perfection by organic dopants in ZTS, ADP and KHP crystals as investigated by high-resolution XRD and SEM Cryst. Growth Des **8**, 446–451 (2008)

12. Y. Zhang, X. Xiaojie, Machine learning band gaps of doped-TiO2 photocatalysts from structural and morphological parameters. ACS Omegax **25**, 15344–15352 (2020)

13. Y. Aoun, B. Benhaoua, S. Benramache, B. Gasmi, Effect of deposition rate on the structural, optical and electrical properties of Zinc oxide (ZnO) thin films prepared by spray pyrolysis technique. Optik **126**, 2481–2484 (2015)

14. G. Viju, T.L. Annusha, S. Sahaya Jude Dhas, A. Panneerselvam, S. Suresh, A.S. Jebamalar, N.S. Nirmala Jothi, A. Jeya Rajendran, Crystal growth, optical, thermal and dielectric properties investigation on cadmium chloride doped L-alanine P-toluene sulfonic acid single crystal for non-linear optical applications. Opt. Quant Electr. **55**, 836 (2023)

15. A. Shiny Febena, M. Victor Antony Raj, J. Madhavan, Systematic investigation and applications of an efficient NLO crystal: glycine lithium sulphate. Mater. Today: Proceed. **8**, 427–434 (2019)

16. S. Prince, T. Suthan, C. Gnanasambandam, Growth and characterization of organic 2,4-dinitroaniline single crystals for optical applications. J. Electron. Mater. **51**, 1639–1652 (2022)

17. M. Meena, B. Samuel Ebinezer, E. Manikandan, R.S. Sundararajan, M. Shalini, R. Natarajan, Synthesis and optical characterizations of l-phenylalanine lithium sulphate (LPLS) semi-organic single crystal. J. Mater. Sci. Mater. Electron. **34**, 395 (2023)

18. M.M. Anne, M.D. Sweetlin, Synthesis and characterization of pure and L-proline doped copper sulphate single crystals. J. Mater. Sci. Mater. Electron. **34**, 974 (2023)

19. M. Meena, M. Shalini, B.S. Ebinezer, R.S. Sundararajan, T.C. Sabari Girisun, E. Manikandan, Investigation on crystal growth, spectral, linear optical studies, and third-order nonlinear optical analysis of L-Cysteine hydrochloride monohydrate lithium sulphate (L-CHMLS) single crystals for optical limiting applications. J. Mater. Sci. Mater. Electron. **34**, 1778 (2023)

20. Y.A.S. Anitha, G. Durgababu, I. Ramakanth, U. Vijayasree, T. Kamalesh, G. Bhagavannarayana, P.V.L. Narayana, Effect of L-histidine hydrochloride monohydrate (LHICL) doping in potassium dihydrogen phosphate (KDP) on single crystal growth, structural, optical, electrical, and mechanical traits. J. Mater. Sci. Mater. Electron. **35**, 594 (2024)

21. K.D. Parikh, D.J. Dave, B.B. Parekh, M.J. Joshi, Thermal, FT-IRand SHG efficiency studies of l-arginine doped KDP crystals. Bull. Mater. Sci. **30**, 105–112 (2007)

22. J.H. Joshi, S. Kalainathan, M.J. Joshi, K.D. Parikh, Influence of L-Serine on micro structural, Spectroscopic, electrical and nonlinear optical performance of ammonium dihydrogen phosphate single crystal. J. Mater. Sci. Mater. Electron. **30**, 14243–14255 (2019)

23. M. Shkir, V. Ganesh, S. AlFaify, H. Algarni, G. Bhagavannarayana, K.K. Maurya, M.M. Abutalib, I.S. Yahia, Bulk growth, structural, vibrational, crystalline perfection, optical and dielectric properties of L-threonine doped KDP single crystals grown by Sankaranarayanan-Ramasamy (SR). Mater. Res. Innov. **21**, 106–114 (2017)

24. G. Durgababu, G. Swati, N. Vijayan, K.K. Maurya, T. Kamalesh, R. Govind Raj, G.J. Nagaraju, G. Bhagavannarayana, Influence of L-Phenylalanine doping on potassium dihydrogen phosphate: crystal growth, structural, optical and mechanical traits. J. Mater. Sci. Mater. Electron. **32**, 5698–5712 (2021)

25. R. Punniyamoorthy, R. Manimekalai, K. Uma, G. Pasupathi, Synthesis and investigation on structural, thermal, mechanical, linear optical, and nonlinear optical nature of potassium sulphato oxalate single crystals. Cryst. Res. Technol. **54**, 1800203 (2019)

26. S.K. Kurtz, T.T. Perry, A Powder Technique for the Evaluation of Nonlinear Optical Materials. J. Appl. Phys. **39**, 3798–3812 (1968)

27. M. Nageshwari, C. Rathika Thaya Kumari, G. Vinitha, S. Muthu, M. Lydia Caroline, Growth and characterization of L-serine: a promising acentric organic crystal. Physica B **541**, 32–42 (2018)

28. N. Rhimi, N. Dhahri, M. Khelifi, E.K. Hlil, J. Dhahri, Structural, morphological, optical and dielectric properties of sodium bismuth titanate ceramics. Inorg. Chem. Commun. **146**, 110119 (2022)

29. A. Yoshikawa, H. Matsunami, Y. Nanishi, Development and applications of wide bandgap semiconductors, in *Wide bandgap semiconductors*. ed. by K. Takahashi, A. Yoshikawa, A. Sandhu (Springer, Heidelberg, 2007), pp.1–24

30. Y. Zhang, X. Xiaojie, Machine learning optical band gaps of doped-ZnO films. Optik **217**, 164808 (2020)

31. M. Rajasekar, K. Meena, K. Muthu, G. Bhagavannarayana, S.P. Meenakshisundaram, Co(II), Co(II)+Mn(II), Co(II)+Ni(II) co-doping effects on tris(thiourea)zinc(II) sulphate crystals: a comparative study. Mol. Cryst. and Liq. Cryst. **623**, 179–193 (2015)

32. P. Anandan, S. Vetrivel, R. Jayavel, C. Vedhi, G. Ravi, G. Bhagavannarayana, Crystal growth, structural and photoluminescence studies of L-tyrosine hydrobromide semi organic single crystal. J. Phys. Chem. Solids **73**, 1296–1301 (2012)

33. G. Bhagavannarayana, P. Rajesh, P. Ramasamy, Interesting growth features in potassium dihydrogen phosphate: unravelling the origin and dynamics of point defects in single crystals. J. Appl. Cryst. **43**, 1372–1376 (2010)

34. D. Jananakumar, P. Mani, J. Therm, Anal. Calorim, Growth and characterization of semiorganic crystal potassium hydrogen oxalate. J. Therm. Anal. Calorim. **115**, 355–359 (2014)

35. B.B. Parekh, P.M. Vyas, S.R. Vasant, M.J. Joshi, Thermal, FT-IR and dielectric studies of gel grown sodium oxalate single crystals. Bull. Mater. Sci. **31**, 143–147 (2008)